scientific reports

Check for updates

OPEN

Validation of a functional human AD model with four AD therapeutics utilizing patterned ipsc-derived cortical neurons integrated with microelectrode arrays

Julbert Caneus[1,4]✉, Kaveena Autar[1,4], Nesar Akanda[1], Marcella Grillo[1], Christopher J. Long[2], Max Jackson[2], Sarah Lindquist[2], Xiufang Guo[1], Dave Morgan[3] & James J. Hickman[1,2]

Preclinical methods are needed for screening potential Alzheimer's disease (AD) therapeutics that recapitulate phenotypes found in the Mild Cognitive Impairment (MCI) stage or even before this stage of the disease. This would require a phenotypic system that reproduces cognitive deficits without significant neuronal cell death to mimic the clinical manifestations of AD during these stages. Long-term potentiation (LTP), which is a correlate of learning and memory, was induced in mature human iPSC-derived cortical neurons cultured on microelectrode arrays utilizing circuit patterns connecting two adjacent electrodes. We demonstrated an LTP system that modeled the MCI and pre-MCI stages of Alzheimer's and validated this functional system utilizing four AD therapeutics, which was also verified utilizing patch-clamp electrophysiology. LTP was induced by tetanic electrical stimulation, and LTP maintenance was significantly reduced in the presence of Amyloid-Beta 42 ($A\beta_{42}$) oligomers compared to the controls, however, co-treatment with AD therapeutics (Donepezil, Memantine, Rolipram and Saracatinib) corrected $A\beta_{42}$-induced LTP impairment. The results illustrate the utility of the system as a validated platform to model MCI AD pathology, and potentially for the pre-MCI phase before significant neuronal death. This system also has the potential to become an ideal platform for high-content therapeutic screening for other neurodegenerative diseases.

Keywords Alzheimer's disease, Long-term potentiation, Human-on-a-Chip, Amyloid-beta42, Drug efficacy, Microelectrode arrays

The majority of prospective new drug candidates show great promise in preclinical studies but fail in clinical trials[1–5]. This disparity can be attributed in part to the dearth of relevant experimental models used during preclinical studies for assessing drug safety and efficacy, especially for Alzheimer's disease (AD)[6,7]. These shortcomings, as they relate to the limitations of biological models, underscore the need to develop better approaches and platforms to improve the drug discovery and development process for AD. To date, animals are the most commonly used models for scientific research and drug screening at the preclinical stage[1]. While animal models are vital and play key roles in basic scientific research and disease understanding, they are, however, limited due to interspecies differences, which can lead to many inconsistencies that affect success for therapeutics in clinical trials[8–11]. For instance, diseases that are associated with APP/Aβ, tau and ApoE dysregulation are affected by several genetic factors, and it can be difficult to establish human-specific disease models using other organisms[12,13]. Thus, more suitable and compatible models that can better replicate complex

[1]NanoScience Technology Center, University of Central Florida, 12424 Research Parkway, Suite 400, Orlando, FL 32826, USA. [2]Hesperos Inc., 12501 Research Pkwy #100, Orlando, FL, USA. [3]Department of Translational Neuroscience, Michigan State University College of Human Medicine, Grand Rapids, MI, USA. [4]Julbert Caneus and Kaveena Autar contributed equally to this work. ✉email: jhickman@ucf.edu

human disease (i.e., physiology and phenotype) and predict drug effects (e.g., toxicity, efficacy) are urgently needed for preclinical drug discovery in AD.

The main pathological features of AD include the formation of extracellular amyloid plaque deposits, intracellular neurofibrillary tangles (NFTs) formed by hyperphosphorylation of tau protein, and a large degree of neuronal cell death and synaptic changes[14]. In addition to Aβ toxicity[15]and tau protein associated toxicity[13,16], other factors that contribute to dementia risk include oxidative stress[17], inflammation[18], cholinergic neuronal damage[19]and neurovascular changes[20], and are based on pathology and genetic risk factors[21]. According to the amyloid hypothesis, the initiating factor in AD is the accumulation and aggregation of the Aβ peptide[22]. Evidence indicates that soluble oligomers of Aβ, including dimers, trimers, dodecamers and spherical aggregates of 6 nm Aβ-derived diffusible ligands (ADDLs) and 12 nm amylospheroids (ASPD)[23]have significantly higher toxicity in vitro than either the monomeric or the larger fibrillar aggregates[24–30]. Moreover, soluble oligomers of Aβ have profound physiological effects at low concentrations even without signs of plaque formation[31–35].

In spite of the significant progress in elucidating the biological mechanisms of AD[36,37], no practical treatments exist that would prevent or significantly delay its progression. This is especially problematic in that by the time symptoms are evident during the mild cognitive impairment (MCI) stage, significant brain neuropathology and even cell death has already occurred[38–40]. Yet, most clinical trials have focused on treating advanced stages of the disease[41,42]. It is now becoming apparent that treatment windows, and thus clinical trials, must shift to the MCI, or better yet the pre-MCI stage, to be effective, however there are few diagnostics, if any, to predict who will develop AD at this stage of the disease[43–45]. Drug discovery can be divided into two general classes—target-based approaches and phenotype-based approaches[46]. Target-based drug discovery has been the most common approach since it is more amenable to the development of high-throughput screening (HTS) assays. The advantage of target-based biochemical and genetic approaches is that large numbers (thousands to millions) of rationally designed compounds can be rapidly screened with today's automated robotic systems in a cost-effective manner. The disadvantages are that multiple positive hits (possibly in the hundreds) targeting single biochemical and genetic pathways are normally identified and no information is obtained from this type of screen on the eventual physiological effect of the compounds at the tissue level. Phenotypic-based drug screens utilize single cells, nematode worms, zebrafish and tissue engineered organ mimics as a primary or secondary in vitro screen for better prediction of which compounds are the best candidates to move into small animal studies[46–50]. These are normally termed High Content Screens (HCS), and include complex Microphysiological systems (MPS), which provide a more holistic analysis of a compound's effects on multiple pathways. While these HCS assays are more labor-intensive and costly than HTS, they are less expensive and more rapid than small animal studies. While HCS assays can be used to reduce the dozens to hundreds of HTS positive hits to a few attractive targets to take into small animal studies, these assays are currently not used as substitutes for whole animal studies, but serve as a bridge between HTS single target assays and in vivo studies. However, recent work utilizing an MPS for a neurodegenerative disease provided efficacy data for C1s complement inhibition to enable a clinical trial application for an autoimmune demyelinating neuropathy, chronic inflammatory demyelinating polyradiculoneuropathy (CIDP) (NCT04658472), and suggests great potential for MPS use for additional translational research leading to IND generation[51]. This also shows MPS systems can be used to generate efficacy data for repurposing drugs or drug candidates without the use of animal data. Long-term potentiation (LTP), in generic terms, refers to long-lasting experience-dependent enhancement of synaptic transmission efficacy, and is considered as the cellular basis of learning and memory. Originally, a large body of LTP studies were conducted through dual electrode patch-clamp electrophysiology in hippocampal slices or in animal models, in which tetanic stimulation at presynaptic sites induced long-lasting potentiation of synaptic transmission (reviewed by[52]). Successful LTP induction was usually demonstrated as an increased excitatory postsynaptic potential (EPSP) upon a regular presynaptic stimulation, and the enhancement of synaptic response lasts from minutes to hours or longer depending on the experimental context[53,54]. Mechanistic investigation indicates high frequency synaptic stimulation, through the opening and mobilization of post-synaptic AMPA receptors, can open NMDA receptors which then triggers a series of downstream signaling pathways including protein expression and gene expression (reviewed by[52,55]). As the importance of LTP as a neuronal functional marker for cognition has been increasingly recognized in the study of dementia and other relevant diseases, its modeling in MEA platforms has started to emerge[56–59] where trains of high frequency stimulation, adapted from an LTP study in rat hippocampal slices[60], can induce an increase of neural activity that lasts at least 1 hour (h). More importantly, blocking of AMPA receptors (with NBQX) and NMDA receptors (with D-AP5), prevents the induction of this activity increase, indicating the long-term activity increase recorded on MEAs is induced via the same signaling cascades as those from classically utilized platforms, confirming their LTP identity, with the former described in our paper in Stem Cell Reports[56].

In this report, we simulated AD pathology in an in vitro system by application of toxic forms of Aβ oligomers and evaluated the functional deficits using circuits of cortical neurons, and identified AD-relevant functional deficits. Previously, we demonstrated that $A\beta_{42}$and tau oligomer application to a cortical neuron MEA platform resulted in pronounced deficits in stimulus-induced neuronal activity from LTP maintenance[61]. To evaluate the system's capacity to assess the effects of AD therapeutics and its potential as a prospective tool in drug development, the systems were treated with $A\beta_{42}$ oligomers and different classes of AD-based drugs, which included Donepezil, Memantine, Rolipram and Saracatinib. These are all either currently approved or in the case of Saracatinib, previously approved but is now withdrawn. Following $A\beta_{42}$ and drug dosing, the functional activity and LTP maintenance of cortical neurons was examined. The results revealed a pronounced decrease in cell activity within 1 h of $A\beta_{42}$ dosing, which was blocked by co-administration of the $A\beta_{42}$ oligomers and AD drugs simultaneously. These results underline the significance and potential of the LTP phenotypic cognitive functional assay system as an applicable tool in the drug development process, which can be employed to quickly analyze promising therapeutic compounds as another metric for efficacy testing of AD therapeutics, but with

only milligrams of a drug candidate. It also provides a tool that can be utilized at the MCI or pre-MCI phases of AD as the deficits in LTP occur without neuronal cell death. Moreover, this system provides a foundation for the development of higher order, highly complex models, which can be used to not only study the drug effects, but also the mechanism of action of potential therapeutics as well.

Results

Analysis of ipsc-derived cortical neurons for the expression of AD drug targets

Currently, Donepezil, Memantine, Saracatinib and Rolipram are all or were FDA-approved drugs utilized for the treatment of AD. Donepezil targets and binds to the acetylcholinesterase enzyme (AChE), subsequently preventing it from catalyzing the hydrolysis of the neurotransmitter acetylcholine (ACh). Memantine binds to the NMDA receptor and blocks the channel from opening and sequentially causes cell excitotoxicity by glutamate. Rolipram inhibits the excessive degradation of cyclic AMP (cAMP) in the presence of $A\beta_{42}$by inhibiting the enzyme phosphodiesterase type 4 (PDE4) that catalyzes its breakdown. The cortical neurons, which had previously been shown to be functionally mature[56], were integrated onto the MEAs in patterns over the microelectrodes. To determine whether the drug targets (e.g., Fyn, NMDAR, AChE, nAChR and PDE4) were expressed in the cortical neurons, the cells were fixed and stained with specific antibodies for each marker followed by microscopy analysis. Figure 1 illustrates neuronal morphology and alignment on patterned MEAs (Fig. 1A,B,E). Additionally, the cells stained positive for all the markers, including Fyn (Fig. 1C), nAChR (Fig. 1D), PDE4 (Fig. 1F), AChE (Fig. 1G), and NMDAR (Fig. 1H).

Analysis of Donepezil treatment on Aβ oligomer induced electrophysiological dysfunction in hipsc-derived cortical neurons

A reduction in acetylcholine neurotransmitters in the brain, due in part to its breakdown and degradation by the acetylcholinesterase enzyme, has been implicated in the development and/or progression of AD pathogenesis[19,62]. Donepezil is an acetylcholinesterase inhibitor therapeutic that has received FDA approval for the treatment of AD[19], and was utilized in this study to evaluate the patterned cortical MEA system's effectiveness in assessing drug effects by changes in electrophysiological properties. To assess the capacity of the system to evaluate drug effects, in parallel experiments, hiPSC-derived cortical neuronal cells were plated on both coverslips and on patterned MEAs and maintained for 28–35 days in culture prior to testing. Patch clamp electrophysiological recordings were preceded by a 24 h acute dose of $A\beta_{42}$oligomers to evaluate individual neuronal cell dynamics according to our previous protocol[61], while MEA experiments investigated 1 h acute responses on LTP maintenance of neuronal population dynamics and synaptic connectivity according to Caneus et al.[61]. On the day of testing, at 24 h post-dose, neuronal function was recorded and analyzed by patch clamp as shown in Fig. 2A–D. The administration of $A\beta_{42}$ oligomers to the cultures resulted in a sharp decrease in cell firing potential. Notably, a significant decrease in sodium currents was observed in cells exposed to $A\beta_{42}$ oligomers compared to $A\beta_{scr}$ oligomer-treated cells (Fig. 2A). Additionally, the data revealed a pronounced reduction and sometimes a complete lack of activity of both action potentials (AP) and spontaneous firing in the cells dosed with $A\beta_{42}$ oligomers relative to samples dosed with $A\beta_{scr}$ oligomers. However, co-treatment with Donepezil (1μM) indicated a clear protection of neuronal function from the effects of $A\beta_{42}$ oligomers, demonstrating statistically significant differences in sodium currents (Fig. 2A) and spontaneous firing amplitude (Fig. 2D).

Similarly, in the hiPSC-derived cortical neuronal MEA systems, the increase in neural activity induced by HFS was able to be maintained at 1 h testing in the $A\beta_{scr}$ control group, abolished in the $A\beta_{42}$ group, but

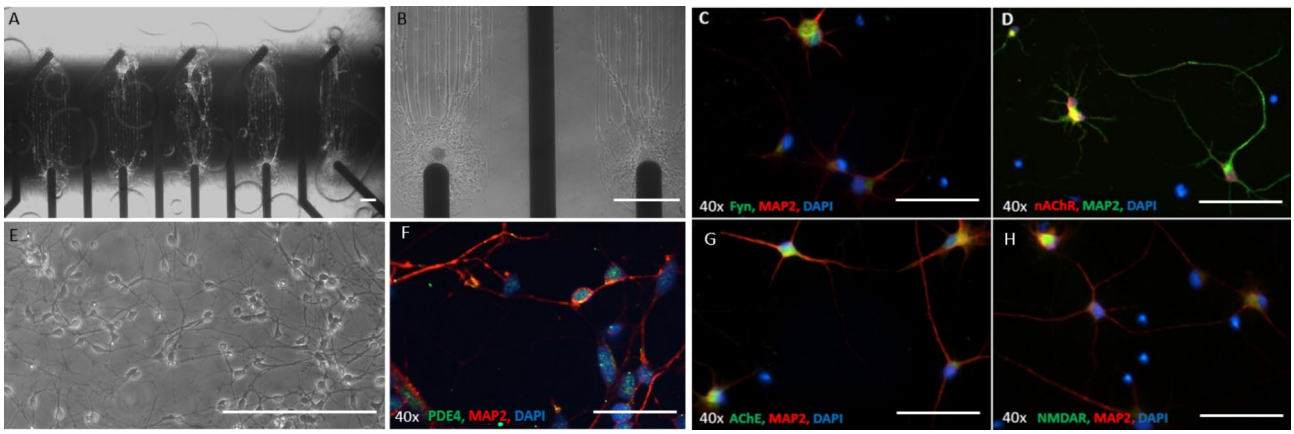

Fig. 1. Morphology of patterned cortical neurons on MEAs and expression of the molecular targets of AD drugs in hiPSC-derived cortical neurons. Phase images of hiPSC-derived cortical neurons distributed on patterns aligned with MEA electrodes (**A**,**B**,**E**), scale bar = 100 μm. (**C**,**D**,**F**,**G**,**H**) Immunocytochemistry of hiPSC-derived cortical neurons utilizing antibodies specific to target proteins relevant for AD drugs revealed the cells expressed all markers evaluated: Fyn (green in **C**), nAChR (red in **D**), PDE4 (green in **F**), AChE (green in **G**), NMDR (green in **H**). Neurons were co-stained with the neuronal marker MAP2 and Dapi in all these images. Scale bar 50 μm.

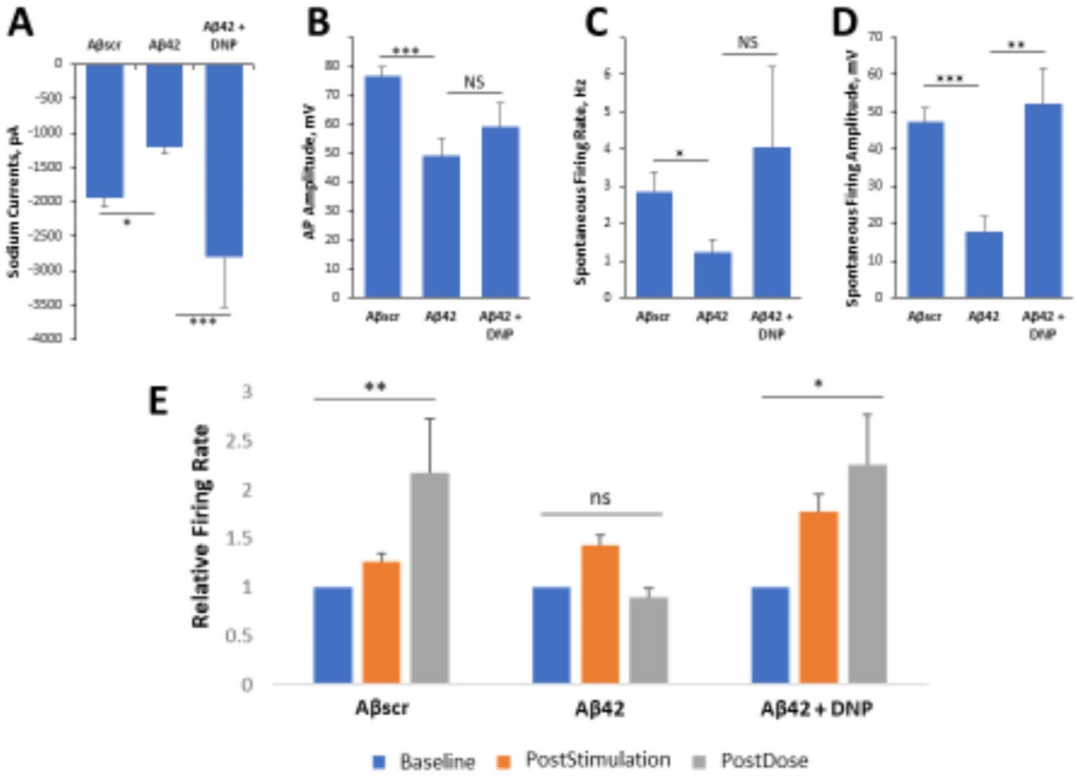

Fig. 2. $A\beta_{42}$ oligomer-induced neurotoxicity of hiPSC-derived cortical neurons is inhibited by Donepezil for both patch clamp and MEA electrophysiological recordings. (**A**–**D**) Patch clamp electrophysiology recordings from the hiPSC-derived cortical neurons indicated the blocking of $A\beta_{42}$-induced deficits by co-treatment with Donepezil (1 μM) for 24 h, as demonstrated for the readouts of sodium currents (**A**), action potential (AP) amplitude (**B**), spontaneous firing rate (**C**) and amplitude (**D**). (**E**) Analysis of cell function on patterned cortical MEA systems revealed a stimulus-induced increase in cell activity (i.e., firing frequency) was maintained in control samples dosed with Aβscr (5 μM), but was completely abolished within 1 h of $A\beta_{42}$ oligomers dosing. However, this $A\beta_{42}$-induced abolishment was blocked by co-treatment with donepezil (DNP, 1 μM). Statistical analysis was performed via one-way ANOVA followed by Fisher's LSD ($\alpha = 0.05$) ($N \geq 16$), $^{*}p \leq 0.05$, $^{**}p \leq 0.01$, $^{***}p \leq 0.001$.

was recovered in the Donepezil group, which demonstrated LTP retention similar to the $A\beta_{scr}$ control group (Fig. 2E). After testing, each MEA system was treated with Lidocaine to confirm that the observed signals were biological in nature and not electronic noise as shown in Fig. S2. This is necessary as electronic noise can resemble AP wave forms depending on the filters employed and the algorithms utilized to analyze the data. After Lidocaine addition, neuronal signals were completely or near-completely abolished (Fig. S2a). The abolishment of neuronal signals within the drug experiments was found to be statistically significant (Fig. S2b), further confirming that all signals used within the analysis for this study were biological. Both the patch clamp and MEA data confirmed the therapeutic effect of Donepezil by blocking the $A\beta_{42}$-induced neurotoxic effects and preserving cell functionality.

To demonstrate that there was functional equivalence between the patch clamp recordings and those obtained with the MEA systems a direct comparison was obtained. Patched cortical neuron traces displayed a marked decrease in cellular activity, including a decrease in sodium and potassium currents (Fig. 3A), lower or lack of induced APs (Fig. 3B) and spontaneous firing (Fig. 3C) in the samples treated with $A\beta_{42}$ oligomers relative to samples treated with $A\beta_{scr}$ or co-treated with $A\beta_{42}$ oligomers and Donepezil at 24 h post-treatment. For the patterned cortical MEA systems, the baseline frequency activity was recorded prior to dosing (Fig. 3D), followed by a HFS pulse to induce LTP (Fig. 3E). Immediately after stimulation and recording, the cells were dosed with $A\beta_{42}$ oligomers with or without Donepezil and incubated for 1 h. LTP induction and maintenance were determined by measuring and comparing cell activity taken immediately after stimulation and at 1 h post-stimulation relative to baseline activity in samples dosed with the $A\beta_{scr}$ control, $A\beta_{42}$oligomers only or in combination with Donepezil. The induced activity was mostly abolished in the $A\beta_{42}$ oligomer treated samples but continued to be maintained in $A\beta_{scr}$ and $A\beta_{42}$ + AD drug treated samples (Fig. 3F). Neuronal activity analysis was confirmed via the addition of 1mM Lidocaine upon completion of LTP testing in Fig. S2. These correlative

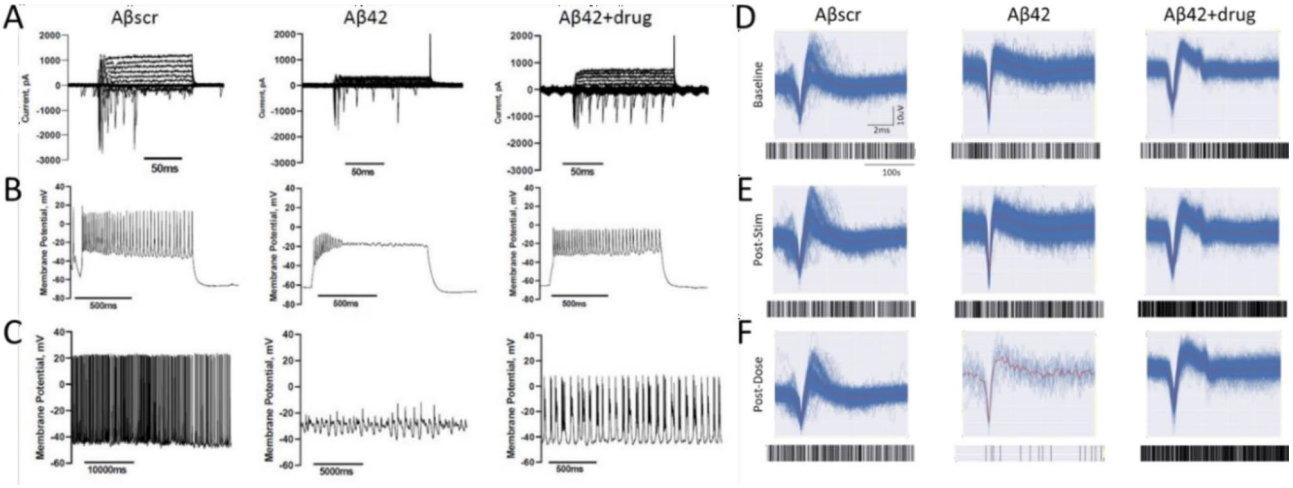

Fig. 3. Correlation of the effects of Donepezil against $A\beta_{42}$ oligomers induced neurotoxicity in cortical neurons utilizing two separate functional measurements. (**A**–**C**) Patch clamp electrophysiology recordings indicated a marked reduction in sodium currents in hiPSC-derived cortical neurons following 5 μM $A\beta_{42}$ oligomer application at 24 h post-treatment (**A**). Additionally, a significant decrease in both induced action potential firing under depolarization (**B**) and spontaneous firing peak amplitudes (**C**) was detected in cells treated with $A\beta_{42}$ relative to cells dosed with amyloid beta scrambled (Aβscr), but the decrease was ameliorated by co-treatment with Donepezil. (**D**–**F**) Similar observations for activity in the parallel cortical MEA systems were identified. Following establishment of baseline activity levels (**D**), increased neural activity was induced by HFS (**E**) followed by different dosing treatment. The increased neural activity was maintained at 1 h post dosing (LTP) in samples treated with $A\beta_{scr}$ (5 μM), but demonstrated a sharp decrease in the samples dosed with $A\beta_{42}$ oligomers alone, however a co-treatment of the $A\beta_{42}$ oligomers and Donepizil rescued the loss of activity (**F**).

measurements indicated the functional equivalence of standard patch clamp analysis of neuronal activity to the MEA neuronal activity obtained for the LTP experiments.

Hipsc-derived cortical neurons retained normal electrical function following co-treatment with ($A\beta_{42}$) oligomers with saracatinib, memantine or rolipram

Saracatinib

To further investigate the neuroprotective effects of AD drugs against $A\beta_{42}$ oligomer neurotoxicity, cells were seeded onto patterned coverslips and treated with Aβ oligomers with or without Saracatinib treatment in parallel experiments with $A\beta_{scr}$ as the control. The neuronal functional activity was measured intracellularly by whole cell patch clamp electrophysiology. Similar to the results in above sections, the addition of $A\beta_{42}$ oligomers to the cortical cultures resulted in prominent cell dysfunction within 24 h post-dosing, and co-treatment with Saracatinib resulted in a blocking of the $A\beta_{42}$ -induced dysfunction in all the parameters analyzed including reduced currents (Fig. 4A), induced action potential amplitude (Fig. 4B) and spontaneous firing rate and amplitude (Fig. 4C,D). To investigate whether Saracatinib offers protective effects against $A\beta_{42}$-induced impairment in LTP, patterned cortical-MEA systems were established and co-treated with Saracatinib together with $A\beta_{42}$ oligomers. The cells were dosed with either $A\beta_{scr}$ or $A\beta_{42}$ oligomers with or without Saracatinib (10 nM) immediately after HFS. As indicated in Fig. 4E, the cells exhibited a significant increase in firing frequency from baseline activity following stimulation. The induced activity was significantly diminished in the samples dosed with $A\beta_{42}$ oligomers relative to $A\beta_{scr}$ treated samples at 1 h post-dosed. However, simultaneous administration of Saracatinib together with $A\beta_{42}$ oligomers inhibited the $A\beta_{42}$-oligomer induced deficits in cell firing and preserved the induced cell activity in the $A\beta_{42}$-Saracatinib treated samples compared to $A\beta_{42}$ only treated samples (Fig. 44E).

Memantine

The effects of Memantine on $A\beta_{42}$-induced cell defects were analyzed by patch clamp electrophysiology and MEA LTP analysis. Based on the results demonstrated in Fig. 5, the application of $A\beta_{42}$ oligomers significantly reduced sodium currents (Fig. 5A), AP amplitude (Fig. 5B), spontaneous firing rate (Fig. 5C), and spontaneous firing amplitude (Fig. 5D), in comparison to samples treated with $A\beta_{scr}$. All of these changes, with the exception of spontaneous firing rate, were significantly counteracted by the co-treatment with Memantine. To assess the protective effects of Memantine on cortical neuronal MEAs they were treated and analyzed as described above. The results demonstrated a marked increase in cell firing frequency from baseline recording following high frequency stimulation (HFS) in all the samples (Fig. 5E). At 1 h after HFS and dosing, this HFS-induced increase was not maintained in the samples treated with $A\beta_{42}$ oligomers, but was in the samples treated with $A\beta_{scr}$ oligomers and those with the co-treatment of $A\beta_{42}$ oligomers and Memantine (Fig. 5E). In all, these findings indicate that Memantine blocked the $A\beta_{42}$-induced neurotoxicity.

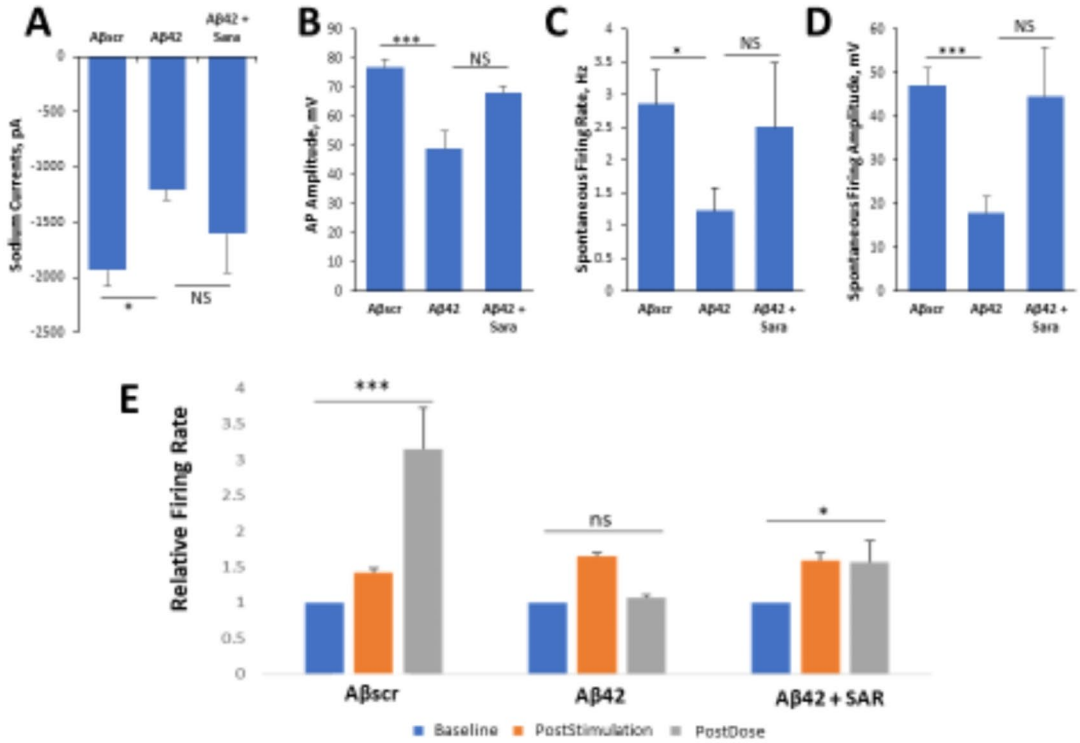

Fig. 4. Saracatinib blocks $A\beta_{42}$ oligomers toxic effects on hiPSC-derived cortical neurons. (**A**–**D**) Patch clamp electrophysiology recordings from the hiPSC-derived cortical neurons showed the blocking of the $A\beta_{42}$-induced defects by co-treatment with Saracatinib (10 nM) for 24 h, as demonstrated for the readouts of sodium currents (**A**), AP amplitude (**B**), spontaneous firing rate (**C**) and amplitude (**D**). (**E**) Analysis of cell function on cortical MEA LTP systems. A stimulus-induced increase in cell activity (i.e., firing frequency) was maintained in control samples dosed with $A\beta_{scr}$ (5 µM), but was completely abolished within 1 h of $A\beta_{42}$ oligomer dosing. However, this $A\beta_{42}$-induced abolishment was blocked by co-treatment with Saracatinib (10 nM). Statistical analysis was performed via one-way ANOVA followed by Fisher's LSD ($\alpha = 0.05$) ($N \geq 25$), $^{*}p \leq 0.05$, $^{**}p \leq 0.01$, $^{***}p \leq 0.001$.

Rolipram

Patch clamp results revealed the potential of Rolipram to prevent neurotoxic effects of $A\beta_{42}$. Though not significant, the co-administration of Rolipram along with $A\beta_{42}$ oligomers for 24 h counteracted the reduction of spontaneous firing rate and amplitude observed in the $A\beta_{42}$ only condition (Fig. 6C,D respectively), while the effect on correcting the reduction of the sodium current is minor (Fig. 6A). Rolipram did, however, significantly block deficits in action potential amplitude (Fig. 6B)[63]. To further evaluate the neuroprotective abilities of Rolipram against $A\beta_{42}$ induced toxicity in LTP, cortical-MEA systems were stimulated and analyzed as described above. Rolipram was observed to have neuroprotective effects, as co-administration of Rolipram with $A\beta_{42}$ oligomers caused a significant increase in event rate at 1 h following LTP induction, comparable to the persistent LTP observed in the $A\beta_{scr}$ treated condition. In contrast, the systems dosed with only $A\beta_{42}$ oligomers had a significant decrease in activity at 1 h post-stimulation (Fig. 6E). Overall, Rolipram was observed to inhibit the neurotoxic effects of $A\beta_{42}$ oligomers in a manner consistent with the mechanism of action of the drug.

Discussion

The drug discovery and development process has been an area of great interest to scientists both in academia and pharmaceutical companies[64–66]. Yet, despite the significantly large investments being dedicated towards this process[67–70], the procedures remain stagnant and inefficient, with less than 15% of all promising new therapeutic compounds receiving marketing approval[3,7]. This paucity is even more striking for neurological disorders[71,72], for instance, as it had been more than 18 years since the last drug was approved for AD treatment, before the recent controversial approval of Aducanumab by the FDA[73–76]. Nevertheless, during that same period, there have been many candidate drugs that showed great promise in preclinical studies but failed in clinical studies[71,77,78]. While there may be many factors that contribute to the high attrition rate of investigative drugs, preclinical models, especially animal models, are believed to be the predominant reason, where efficacy (52%) or

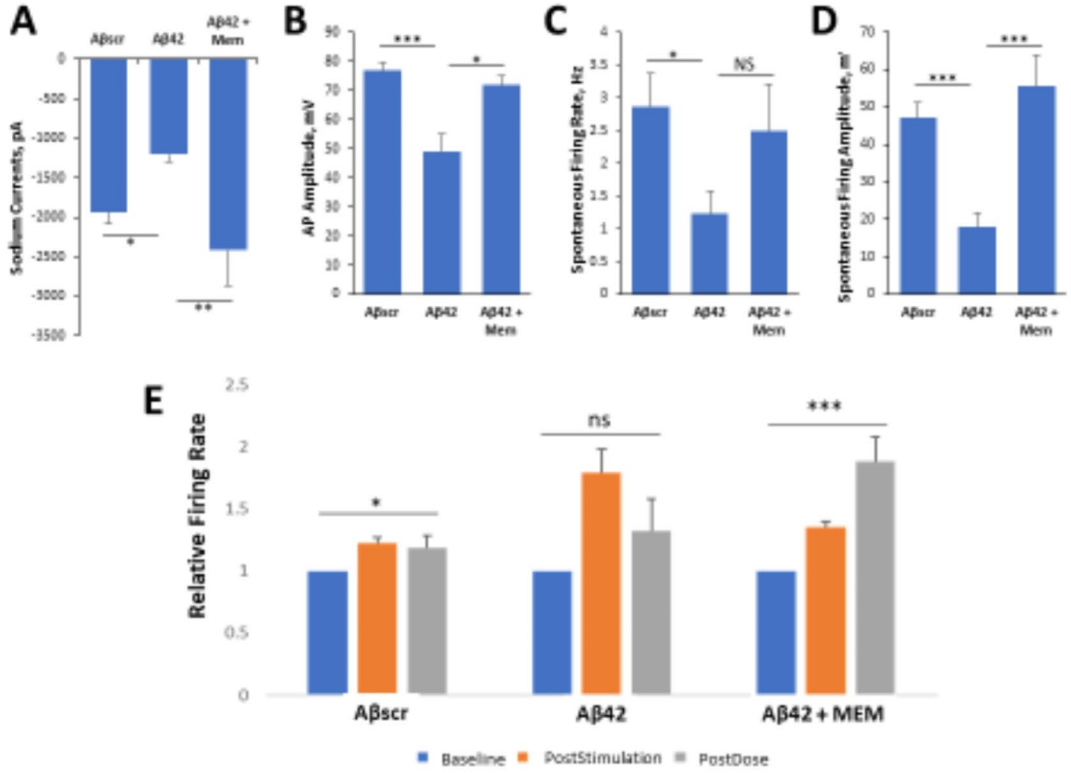

Fig. 5. Memantine suppresses $A\beta_{42}$ oligomers neurotoxic effects on hiPSC-derived cortical neurons. (**A**–**D**) Patch clamp electrophysiology recordings from the hiPSC- derived cortical neurons show the blocking of $A\beta_{42}$-induced defects by co-treatment with Memantine (5 µM) for 24 h, as demonstrated for the readouts of Sodium currents (**A**), AP amplitude (**B**), spontaneous firing rate (**C**) and amplitude (**D**). (**E**) Analysis of cell function on cortical MEA LTP systems, indicated a stimulus-induced increase in cell activity was maintained in control samples dosed with $A\beta_{scr}$ (5 µM), but was completely abolished within 1 h of $A\beta_{42}$ oligomers dosing. However, this $A\beta_{42}$-induced abolishment was blocked by co-treatment with memantine (5 µM). Statistical analysis was performed via one-way ANOVA followed by Fisher's LSD ($\alpha = 0.05$) ($N \geq 25$), $^{*}p \leq 0.05$, $^{**}p \leq 0.01$, $^{***}p \leq 0.001$, $^{****}p \leq 0.0001$.

safety (24%) account for the majority of drug failures in clinical trials[79]. Historically, the drug discovery process has relied largely on animal models for safety and efficacy research in order to obtain preclinical evaluation of promising new therapeutic compounds[6,80,81]. However, the genetic differences between animals and humans is regarded as one of the main factors contributing to the very high attrition rate in human studies[1,6,11]. The lack of compatible models to study human diseases has greatly impeded the drug development process.

Recent advances in the development and differentiation of hiPSCs into mature cells now provide a new source and endless possibilities to create more relevant models[82]. Today, based on the relative ease with which different types of human cells (especially neuronal cells, which are normally inaccessible for scientific research prior to death) can be generated from hiPSCs, many researchers are re-evaluating their research approaches and putting more emphasis towards developing compatible, hiPSC-derived in vitro models to study human diseases and for drug development[83]. Previously, we generated a human-based system using cortical neurons derived from iPSCs to study aspects of AD pathophysiology without neuronal death[61]. Here, using four AD-related drugs, the system's capacity was investigated as a potential platform for drug screening for AD, more specifically for mild cognitive impairment (MCI). This is important as there are few, if any, screens for the MCI, or pre-MCI, stages of the disease, which this system can address. As indicated in the results above, a significant increase in cell firing frequency from baseline activity was detected in the system following stimulation using a HFS protocol. This HFS-induced increase was maintained at least for 1 h and is defined as LTP, which is a correlate for learning and memory[61]. The stimulus-induced change in cell activity was subsequently abolished by $A\beta_{42}$ oligomer dosing while preserved in the $A\beta_{scr}$ group, but without cell death.

Both Donepezil and Memantine have been approved by the FDA as separate or a combined (Namzaric) drug for AD treatment[84]. Both drugs, as well as Rolipram and Saracatinib, were evaluated independently in this cortical neuron AD platform. The $A\beta_{42}$ oligomers' neurotoxic effect was inhibited in the presence of the AD-related drugs, demonstrating the system proficiency to capture $A\beta_{42}$ induced functional deficits and their rescue

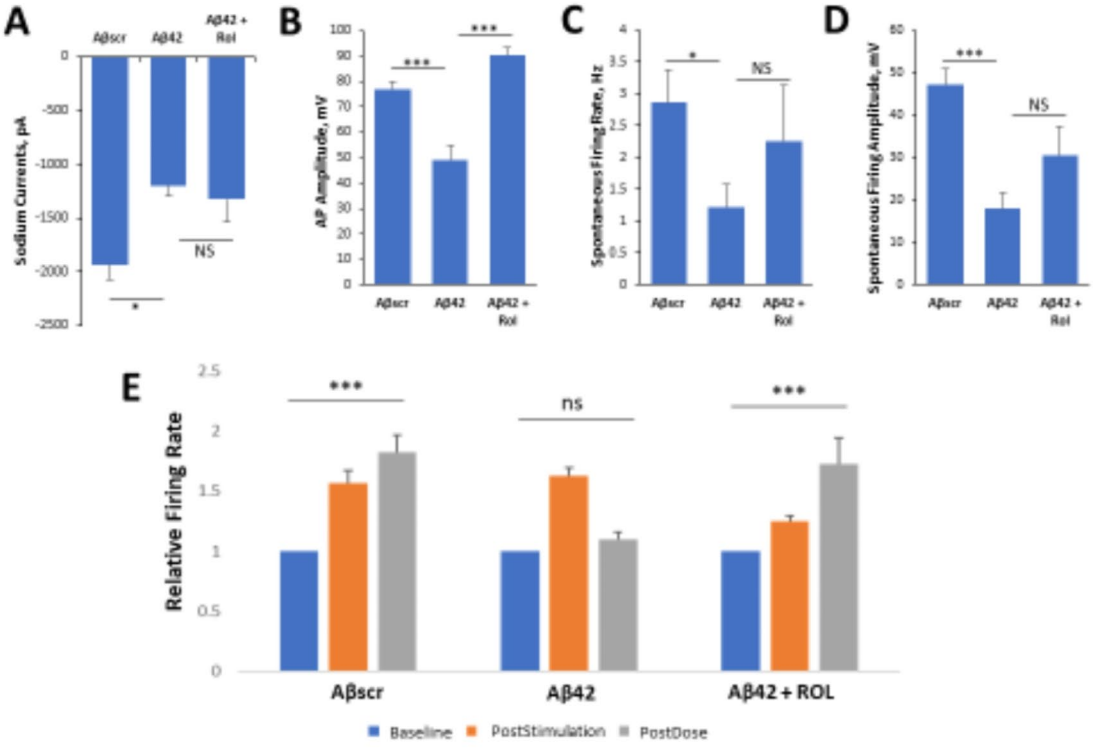

Fig. 6. Rolipram suppresses $A\beta_{42}$ oligomer neurotoxic effects on hiPSC-derived cortical neurons. (**A–D**) Patch clamp electrophysiology recordings from the hiPSC-derived cortical neurons showed the blocking of the $A\beta_{42}$-induced defects by co-treatment with Rolipram (1 μM) for 24 h, as demonstrated for the readouts of sodium currents (**A**), AP amplitude (**B**), spontaneous firing rate (**C**) and amplitude (**D**). (**E**) Analysis of cell function on cortical-MEA systems showed a stimulus-induced increase in cell activity was maintained in control samples dosed with $A\beta_{scr}$ (5 μM), but was completely abolished within 1 h of $A\beta_{42}$ oligomer dosing. This $A\beta_{42}$-induced abolishment was blocked by co-treatment with Rolipram (1 μM). Statistical analysis was performed via one-way ANOVA followed by Fisher's LSD ($\alpha = 0.05$). ($N \geq 18$), $^{*}p \leq 0.05$, $^{**}p \leq 0.01$, $^{***}p \leq 0.001$, $^{****}p \leq 0.0001$.

by the tested drug. Patch clamp recordings evaluated individual neuron electrophysiological activity, while MEA experiments investigated the LTP maintenance in the neural populations for dynamic circuit activity and active synaptic interactions. We observed intra- and inter-batch variability concerning the amplitude of LTP in control conditions and the effect of $A\beta_{42}$. This variability reflects a limitation of all the iPSC-derived models due to their high dependence on the quality consistency of large collection of biological factors. Despite this, solid conclusions can still be drawn with the number of replicates and statistical analysis. In brief, this study supports our previous work demonstrating the validity of these two protocols in inducing and evaluating AD-relevant phenotypes[61] as well as their validity for testing AD therapeutics.

There are many mechanisms that produce synaptic plasticity for both excitatory and inhibitory synapses[85]. Our LTP protocol induces an increase in neuronal firing rates with short bursts of high frequency stimulation, often employed in slices to produce LTP at glutamatergic synapses in the Schaffer collateral system of the hippocampus. Although we have previously demonstrated this increased activity is dependent on AMPA receptor activity as detailed in our publication in Stem Cell Reports[56], also featured in Fig. 3, we make no specific claims regarding the mechanisms by which this is achieved, only that it is a form of plasticity induced by an LTP producing stimulus. While more studies are needed to expand on the findings presented here, and to further validate the effectiveness and applicability of the system as a platform for drug screening, the findings, nonetheless, provide evidence to support the utility of the system as a more relevant human-based in vitro system to model AD at the preclinical stage, especially for the MCI stage of the disease.

These Human-on-a-Chip systems are potentially significant for a number of important reasons: (1) they provide a human-based in vitro model to study disease pathophysiology (i.e., mechanisms and pathways) in vitro; (2) they provide a simple, reproducible and economically effective tool for drug screening (e.g., toxicity and efficacy); (3) they provide a foundation for designing and creating more complex systems that can be used to study the mechanism of drug reaction, the mode of transport and to screen libraries of already approved drugs for drug repurposing; (4) they are scalable, and can be used for high-content drug testing; and (5) they can be used in the application of personalized medicine. Data generated with these models can also provide

support for INDs to repurpose existing drugs as indicated by a previous study for testing C1s complement inhibition in CIDP (NCT04658472), which suggests great potential for MPS systems use for translational research leading to IND generation[51]. Despite the connection of Aβ accumulation to AD, it is now accepted that the amyloid plaques are not sufficient to cause the symptoms of AD. It appears that in addition to Aβ, there is a requirement for the spread of tau pathology throughout the brain regions critical for learning and memory before the disease becomes manifest. Experimental studies in transgenic mice suggest that addition of Aβ to mouse models of tauopathy can exacerbate the amount of tau deposition and accelerate the development of the AD phenotype[86,87]. Importantly, while murine models of amyloid pathology generally fail to result in major neuronal loss[88,89], murine tau models have extensive neuronal loss and brain atrophy[90,91]. It is also recognized that the amount of tau pathology is more closely associated with the extent of cognitive decline in older adults and AD cases than the amount of amyloid pathology[92]. The dual impacts of amyloid and tau on neural function also enable the evaluation of each of these as possible initiators of peripheral nervous system changes found in AD[93,94]. In light of tau's significant effects on AD, future studies will utilize the LTP platforms to investigate this important variable in AD pathology.

Conclusion

This study validated the ability of a human based iPSC-derived cortical neuron-MPS platform to model cognitive dysfunction for AD drug testing, utilizing patterned cortical neurons on MEAs to enable LTP as a functional cognitive marker without cell death. This point is important as cell death begins to occur in AD as soon as the MCI stage and is as much as 40–60% in advanced stages of the disease. This provides a relevant model for MCI or even pre-MCI evaluation of therapeutic candidates. Each of the four drugs utilized: Donepezil, Memantine, Saracatinib, and Rolipram, was able to successfully block $A\beta_{42}$-oligomer induced functional deficits as indicated by LTP preservation and confirmed by whole-cell patch clamp electrophysiology. This model can be applied to pre-clinical drug evaluation for AD as well as for other cognitive deficits after proper adaptation for frontotemporal dementia, Lewy body disease or for other neurological conditions.

Methods

Study design

This project aimed to validate an hiPSC-derived cortical neuron system for monitoring AD-relevant functional deficits to enable the evaluation of the effectiveness of AD therapeutics. Two functional assays were employed: patch clamp electrophysiology analysis on neurons cultured on coverslips and LTP analysis of neural circuits cultured on patterned MEAs. To evaluate the response of Aβ oligomer treatment, cells on coverslips were treated with the $A\beta_{42}$ oligomers, control scrambled Aβ oligomers ($A\beta_{scr}$), or $A\beta_{42}$ oligomers plus AD therapeutics for 24 h and then subjected to patch clamp analysis. Neuronal MEAs were recorded at baseline activity, immediately after high frequency stimulation (HFS) for LTP induction, then treated with $A\beta_{42}$ oligomers, $A\beta_{scr}$, or $A\beta_{42}$ oligomers plus AD therapeutics, and recorded again at 1 h post-HFS for LTP-quantification. For patch clamp electrophysiology, the parameters analyzed were: amplitude of the sodium current, amplitude of the action potentials (AP), number of spontaneous firings within a 30 s duration, and amplitude of spontaneous firing. For the MEA assay, the parameter analyzed was the neural activity at 1 h post LTP induction normalized by baseline activity. For each drug evaluated, there were three experimental groups: cells treated with $A\beta_{scr}$ as the control, those treated with $A\beta_{42}$ oligomers as the AD pathological group, and those treated with $A\beta_{42}$ oligomers plus AD drug as the therapeutically treated group. The AD deficit was evaluated by comparing between the $A\beta_{42}$ group and the control, and the drug's effect was evaluated by comparing between the $A\beta_{42}$ + drug group with the $A\beta_{42}$ group. The number of systems tested was determined statistically so as to detect a significant difference between the $A\beta_{42}$ group and the control, with a type I error rate (α) of 0.05.

Neural cells

Human cortical neurons were used to assess the effects of multiple classes of AD therapeutics on Aβ oligomer induced neuronal cell dysfunction. The cells were derived from human iPSCs from healthy individuals and were either purchased from Cellular Dynamics International (CDI, iCell GlutaNeurons, Cat. #: C1033, Madison, WI) or differentiated directly in our lab as described previously[56,61,95]. Human primary astrocytes were purchased from ScienCell (Cat. # 1800).

Surface chemistry

Neuronal surface patterning on custom MEA chips was prepared using a surface coating protocol of polyethylene glycol (PEG), followed by laser ablation and backfill coating with DETA (*N*-1(3-[trimethoxysilyl]propyl)-diethylenetriamine) as detailed in Wilson et al.[96]. Subsequently, neuronal attachment was further encouraged with a protein adsorption coating of poly-L-ornithine (PLO) and laminin, which consisted of a 1 h RT incubation of 0.01% PLO solution, followed by 3X rinses of 1X PBS before incubating overnight at 4 °C with 10 µg/ml laminin solution[56]. The laminin solution was removed prior to cell seeding.

Cell culture

The cells were seeded on the patterned MEA surfaces and on coverslips. A monoculture of cortical neurons were plated at a density of 150 cells/mm^2on coverslips for immunostaining (ICC) analysis and patch clamp electrophysiology as described previously[34,61]. For the MEA cultures, a co-culture of cortical neurons and astrocytes were seeded directly onto patterned MEAs to promote cell adhesion of separated cell-clusters on the individual electrodes, as well as the formation of synaptic connections between two adjacent electrodes. The neuronal cells were plated at a density of 500 cells/mm^2 and the astrocytes at 250 cells/mm^2. The cells were

first plated in the manufacture's (CDI) recommended medium for the first 24 h before they were switched to a serum-free medium. The cells were maintained in culture in the serum-free medium for 28–35 days prior to dosing and testing[61].

Aβ oligomer preparation

The Aβ oligomers were prepared using peptides from rPeptide ($A\beta_{1\text{-}42}$ catalog number A-1002-2; $A\beta_{scrambled}$A-1004-2) as described previously[97]. First, the peptides were re-suspended in 500 µL of HFIP (catalog number AC445820100; Fisher Scientific) and left to dry overnight under a ventilated hood. The next day the samples were spun in a SpeedVac until dry and stored desiccated at -20 °C until use. Prior to using, the solution was sonicated for 5 min and centrifuged at 1400 x g for 5 min.

Preparation of AD drugs

Several classes of drugs used in the treatment of AD were used in this study, including Rolipram (Cayman Chemicals, Cat. # 10011132), Saracatinib (Cayman Chemicals, Cat. # 379231-04-6), Memantine (Cayman Chemicals, Cat # 14184) and Donepezil (Sigma, Cat. # D6821). Memantine is an uncompetitive N-methyl-D-aspartate (NMDA) receptor antagonist that binds to the receptor and blocks the binding of glutamate and thus cell excitotoxicity caused by glutamate[98]. Donepezil is an FDA-approved drug for AD, it is an acetylcholinesterase inhibitor that prevents the breakdown of acetylcholine in the synapse by the acetylcholinesterase enzyme[99,100]Saracatinib inhibits the action of Fyn, a member of the tyrosine kinase family that phosphorylates other proteins including tau and NMDAR, resulting in tau hyperphosphorylation and synaptic toxicity/or cell excitotoxicity from NMDAR activation[101–104]. Rolipram is a selective phosphodiesterase-4 (PDE4) inhibitor that helps to restore the cAMP level which is affected (i.e., reduced) in AD as a result of adenylate cyclase (synthesizes cAMP) inactivation by $A\beta_{42}$peptides[105]. All drug stocks were prepared by reconstitution in 1X PBS.

Drug treatment of cortical neurons

Neuronal cultures were treated for patch clamp via half medium exchange containing either $A\beta_{scr}$ or $A\beta_{42}$ oligomers with or without AD drugs 24 h prior to testing. For MEA analysis, cells were fed at 24 h prior to treatment by performing a half medium change to prepare the cells for the intensive activity testing the next day. Upon testing time, following the 5 min baseline testing, LTP induction and 5 min recording right after the induction, the cells were either dosed with a final concentration of 5 µM $A\beta_{scr}$, 5 µM of $A\beta_{42}$ alone, or 5 µM of $A\beta_{42}$ plus drug (either 10 nM of Saracatinib, 1 µM of Donepezil, 5 µM of Memantine, or 1 µM of Rolipram). To examine the neurotoxic effects of $A\beta_{42}$ oligomers on cell electrophysiological function, the cells or cultures were tested at 1 h (MEAs) following treatment by conducting another 5 min recording. At the end of the activity testing, a dose of 1mM Lidocaine was always applied to silence all the neural activity so as to confirm the biological source of the recorded signals. Those signals that were not abolished by lidocaine were considered as noise and were excluded from MEA analysis.

Immunocytochemistry and confocal microscopy

To analyze the cells for gene expression of the drug targets, the cells were fixed in 4% paraformaldehyde (PFA), followed by cell permeabilization and incubation in primary and secondary antibodies solutions (diluted in BSA/NGS/T20 buffer) for each specific marker. Following antibody staining, the cells were counterstained with DAPI (4',6-diamidino-2-phenylindole) and mounted on glass slides for analysis. The cells were imaged using a confocal microscopy (Zeiss, Axioskop 2, Germany). The following primary antibodies (at 1/1000 dilution) were used: Rabbit Anti-Microtubule-Associated Protein 2 (Millipore, Cat. #: AB5622), Mouse Anti-MAP2 (Abcam, Cat. #: ab11257), Mouse Anti-Fyn (ThermoFisher, Cat. #: MA1-15865), Mouse Anti-NMDAR2B (ThermoFisher, Cat. #: MA1-2014), Mouse Anti-Acetylcholinesterase (Abcam, Cat. #: ab2803), Mouse Anti-muscarinic Acetylcholine Receptor (Abcam, Cat. #: ab90805), Rabbit Anti-nicotinic Acetylcholine Receptor (Abcam, Cat. #: ab221868), Rabbit Anti-Phosphodiesterase Type 4 (Abcam, Cat. #: ab14628). The secondary antibodies used: Alexa-Fluor 488 goat anti-rabbit (ThermoFisher, Cat. # A11008), AlexaFluor 488 Goat anti-mouse (ThermoFisher Cat. #: A11001), AlexaFluor 568 Goat anti-Rabbit (ThermoFisher Cat. #: A11036), and AlexaFluor 568 Goat anti-mouse (ThermoFisher Cat. #: A11004).

Patch clamp electrophysiology recording of cortical neurons

To measure individual neuronal activity, whole cell patch clamp recordings were taken using a Zeiss, upright microscope (Axioscope, FS2, Carl Zeiss, Germany) equipped with a multiclamp 700B amplifier and an intracellular solution consisting of 140 mM K-gluconate, 4 mM NaCl, 0.5 mM $CaCl_2$, 1 mM $MgCl_2$, 1 mM EGTA, 5 mM HEPES Acid, 5 mM HEPES base and 5 mM Na_2ATP as described previously[61]. Depolarization-evoked inward and outward currents were examined in voltage-clamp mode while induced action potentials (APs) were recorded in current-clamp mode. Successive analysis of the data was carried out using pClamp 10 software (Axon Instrument, Foster City, CA, USA) followed by quantification using Microsoft Excel and GraphPad Prism. For only the patch clamp data, data across experiments for $A\beta_{42}$ and $A\beta_{scr}$ were separately pooled to better represent the differential effects.

Analysis of cortical neuron firing activity on MEAs

The cellular activity of the cells was measured extracellularly on MEAs as described previously[34,59,61]. The cells were plated directly onto the MEAs in housing and maintained in culture for 28–35 days before LTP experiments with Aβ oligomers and AD drugs. Prior to treatment, spontaneous activity (baseline) of the neurons was recorded (for 5 min) followed immediately by high frequency electrical stimulation (LTP induction) and another 5 min recording post-stimulation. Immediately following LTP induction and recording, the cultures were treated with

Aβ oligomers or Aβ oligomers with AD drugs and incubated for 1 h at 37 °C and 5% CO_2. Next, the neuronal firing (e.g., firing frequency) was once again recorded for 5 min before analysis. The data was analyzed using the Anaconda distribution of Python software.

Long term potentiation induction on MEAs and post-processing analysis

To induce LTP on cortical neurons cultured on MEAs, a high frequency stimulation (HFS) protocol was used as described previously[61]. Test stimuli were delivered to all the electrodes in the form of 80 pulses at 100 Hz. The evoked response or induced cell activity was then analyzed using the Anaconda distribution of Python software. Following the isolation of template shapes, a high-pass filter (100 Hz), standard deviation cross, template matching, and principal component analysis was utilized. Raw electrode data recorded from customized MEA chips was filtered using a Butterworth 2nd order 100 Hz high-pass filter. Spikes occurring at the same microsecond on more than two electrodes were deemed as artifacts and removed. It has been observed that transient noise effects tend to co-occur simultaneously across multiple electrodes, whereas coupled biological events (such as co-firing neurons) co-occur at timestamps that are very close, but which are not identical to each other. The waveforms (e.g., action potential spikes and frequency) were thresholded at − 5 standard deviations from the noise. Any electrodes with firing frequency post-stimulation less than or equal to baseline levels were excluded from the data analysis. 1 mM Lidocaine was utilized as a confirmation of biological signal, and was shown to abolish neuronal activity within 1 min of addition (Fig. S2). Extensive detailing on signal processing is described in Autar et al.[56].

Statistical analysis

All data is comprised of data collected from at least 3 independent experiments with at least 3 replicates per experiment. A replicate (N) has been defined as a patched cell for whole-cell patch clamp electrophysiology, or an MEA electrode for LTP experiments. Comparison of the mean of at least three or more replicates and more than 15 electrodes between groups was performed. For computational analyses, Microsoft Excel software and GraphPad Prism were used. One-way analysis of variance (ANOVA) followed by a multiple comparisons test (Fisher's LSD) was performed for comparison across multiple experimental groups. Student's t-tests were used for statistical comparison analysis between two experimental groups. Error bars represent standard error of the mean, and in all statistical tests, $\alpha = 0.05$.

Data availability

Data is provided within the manuscript or supplementary information files. The datasets are available from the corresponding author on reasonable request.

Received: 23 April 2024; Accepted: 23 September 2024
Published online: 22 October 2024

References

1. Van Norman, G. A. *JACC Basic. Transl Sci.*, **4**, 845–854. (2019).
2. Hay, M., Thomas, D. W., Craighead, J. L., Economides, C. & Rosenthal, J. *Nat. Biotechnol.* 40–51. (2014).
3. Wong, C. H., Siah, K. W. & Lo, A. W. *Biostatistics*, **20**, 273–286. (2019).
4. Munro, H. D. J. *Nature*, 495–496. (2019).
5. Clinicaltrials.Gov *NIH - US National Library of Medicine*, (2021).
6. Atkins, J. T. et al. *Br. J. Cancer*, 1496–1501. (2020).
7. Dowden, H. & Munro, J. *Nat. Rev. Drug Discov* **18**, 495–496. (2019).
8. Huang, Y. et al. *Microphysiological Syst.*, **4**. (2020).
9. Pound, P. & Ritskes-Hoitinga, M. *J. Transl Med.* **16**, 304. (2018).
10. Perel, P. et al. *BMJ*, **334**, 197. (2007).
11. Geerts, H. *CNS Drugs*, 915–926. (2009).
12. Cummings, J. L., Vinters, H. V., Cole, G. M. & Khachaturian, Z. S. *Neurology*, **51**, S2–17 ; (1998). discussion S65-7.
13. Chen, X. Q. & Mobley, W. C. *Front. Neurosci.* **13**, 659. (2019).
14. Lee, J. C., Kim, S. J., Hong, S. & Kim, Y. *Exp. Mol. Med.* **51**, 53–53. (2019).
15. Jucker, M. & Walker, L. *Nature*, **525**, 193–194. (2015).
16. Bloom, G. *JAMA Neurol.* **71**, 505–508. (2014).
17. Tönnies, E. & Trushina, E. *J. Alzheimers Dis.* **57**, 1105–1121. (2017).
18. Azizi, G. & Mirshafiey, A. *Immunopharmacol. Immunotoxicol* **34**, 881–895. (2012).
19. Hampel, H. et al. *Brain*, **141**, 1917–1933. (2018).
20. Klohs, J. *Neurodegener Dis.* **19**, 109–127. (2019).
21. O'connell, K. M. S., Ouellette, A. R., Neuner, S. M., Dunn, A. R. & Kaczorowski, C. C. *Genes Brain Behav.* **18**, e12603 (2019).
22. Selkoe, D. J. & Hardy, J. *EMBO Mol. Med.* **8**, 595–608. (2016).
23. Huang, Y. R. & Liu, R. T. *j. Mol. Sci.* **21**, 4477. (2020).
24. Deshpande, A., Mina, E., Glabe, C. & Busciglio, J. *J. Neurosci.* **26**, 6011–6018. (2006).
25. Hoozemans, J. J. M., Chafekar, S. M., Baas, F., Eikelenboom, P. & Scheper, W. *Curr. Med. Chem.* **13**, 2599–2605. (2006).
26. Lambert, M. P. et al. *Proc. Nat. Sci. USA*, *95*, 6448–6453 (1998).
27. Paranjape, G. S., Gouwens, L. K., Osborn, D. C. & Nichols, M. R. *ACS Chem. Neurosci.* **3**, 302–311. (2012).
28. Sengupta, U., Nilson, A. N. & Kayed, R. *EBioMedicine*, **6**, 42–49. (2016).
29. Caughey, B. & Lansbury, P. T. *Annu. Rev. Neurosci.* **26**, 267–298. (2003).
30. El-Agnaf, O. M. A., Mahil, D. S., Patel, B. P. & Austen, B. M. *Biochem. Biophys. Res. Commun.* **273**, 1003–1007. (2000).
31. Hartley, D. M. et al. *J. Neurosci. Methods*, **19**, 8876–8884. (1999).
32. Stefani, M. & Dobson, C. M. *J. Mol. Med.* **81**, 678–699. (2003).
33. Walsh, D. M. & Selkoe, D. J. *Neuron*, **44**, 181–193. (2004).
34. Varghese, K. et al. *PLoS One*, **5**, e8643. (2010).
35. Berry, B. J., Smith, A. S. T., Long, C. J., Martin, C. C. & Hickman, J. J. *ACS Chem. Neurosci.* **9**, 1693–1701. (2018).
36. Dá Mesquita, S. et al. *Neurosci. Biobehav Rev.* **68**, 547–562. (2016).

37. Frozza, R. L., Lourenco, M. V. & De Felice, F. G. *Front. Neurosci.* **12**, 37–37. (2018).
38. Gómez-Isla, T. et al. *J. Neurosci.* **16**, 4491–4500. (1996).
39. Markesbery, W. R. et al. *Arch. Neurol.* **63**, 38–46. (2006).
40. Price, J. L., Davis, P. B., Morris, J. C. & White, D. L. *Neurobiol. Aging*, **12**, 295–312. (1991).
41. Cummings, J., Lee, G., Ritter, A., Sabbagh, M. & Zhong, K. *Alzheimers Dement. (N Y)*, **5**, 272–293. (2019).
42. Cummings, J., Lee, G., Ritter, A. & Zhong, K. *Alzheimers Dement. (N Y)*, **4**, 195–214. (2018).
43. Bjerke, M. & Engelborghs, S. *J. Alzheimers Dis.* **62**, 1199–1209. (2018).
44. Blennow, K. & Zetterberg, H. *J. Intern. Med.* **284**, 643–663. (2018).
45. Tamaoka, A. *Brain Nerve*, **72**, 23–34. (2020).
46. Terstappen, G. C., Schlupen, C., Raggiaschi, R. & Gaviraghi, G. *Nat. Rev. Drug Discov* **6**, 891–903. (2007).
47. Burkhardt, M. F. et al. *Mol. Cell. Neurosci.* **56**, 355–364. (2013).
48. Peppard, J. V. et al. *J. Biomol. Screen.* **20**, 382–390. (2015).
49. Subramanian, B. et al. *Tissue Eng. Part. A*, **16**, 2821–2831. (2010).
50. Sun, N. et al. *Sci. Transl Med.* **4**, 130ra47. (2012).
51. Rumsey, J. W. et al. *Adv. Ther. (Weinh)*, **5**, 2200030. (2022).
52. Nicoll, R. A. *Neuron*, **93**, 281–290. (2017).
53. Abbas, A. K., Villers, A. & Ris, L. *Rev. Neurosci.* **26**, 507–546. (2015).
54. Malenka, R. C., Kauer, J. A., Perkel, D. J. & Nicoll, R. A. *Trends Neurosci.* **12**, 444–450. (1989).
55. Lüscher, C. & Malenka, R. C. *Cold Spring Harb Perspect. Bioldoi*, **4**, a005710. (2012).
56. Autar, K. et al. *Stem Cell. Rep.*, **17**, 96–109. (2022).
57. Odawara, A., Katoh, H., Matsuda, N. & Suzuki, I. *Biochem. Biophys. Res. Commun.* **469**, 856–862. (2016).
58. Pré, D. et al. *Stem Cell. Rep.*, **17**, 2141–2155. (2022).
59. Edwards, D. et al. *ACS Biomater. Sci. Eng.* **3**, 3525–3533. (2017).
60. AbrahamA, W. C. & Huggett *Hippocampus*, **7**, 137–145. (1997).
61. Caneus, J. et al. *Alzheimers Dement. (N Y)*, **6**, e12029. (2020).
62. Ferreira-Vieira, T. H., Guimaraes, I. M., Silva, F. R. & Ribeiro, F. M. *Curr. Neuropharmacol.* **14**, 101–115. (2016).
63. Lee, D. *Front. Pharmacol.* **6**, 161–161. (2015).
64. Adams, C. P. & Brantner, V. V. *Health Aff (Millwood)*, **25**, 420–428. (2006).
65. Dahlin, E., Nelson, G. M., Haynes, M. & Sargeant, F. *J. Clin. Pharm. Ther.* **41**, 198–202. (2016).
66. Shih, H. P., Zhang, X. & Aronov, A. M. *Nat. Rev. Drug Discov* **17**, 19–33. (2018).
67. Wouters, O. J., Mckee, M. & Luyten, J. *JAMA*, **323**, 844–853. (2020).
68. Dimasi, J. A., Grabowski, H. G. & Hansen, R. W. *J. Health Econ.* **47**, 20–33. (2016).
69. Dierynck, B. & Joos, P. *JAMA*, **324**, 516–517. (2020).
70. Waring, M. J. et al. *Nat. Rev. Drug Discov* **14**, 475–486. (2015).
71. Cummings, J. L., Morstorf, T. & Zhong, K. *Alzheimers Res. Ther.* **6**, 37. (2014).
72. Clinicaltrials.Gov *List of Alzheimer related drugs in clinical trials.*
73. Alzforum. https://www.alzforum.org/therapeutics/memantine.
74. Mullard, A. *Nature* (2021).
75. Knowles, J. *Core Evid.*, **1**, 195–219. (2006).
76. Reisberg, B. et al. *NEJM*, 1333–1341. (2003).
77. Cummings, J., Lee, G., Ritter, A., Sabbagh, M. & Zhong, K. *Alzheimers Dement. (N Y)*, **6**, e12050. (2020).
78. Mullane, K. & Williams, M. *ScienceDirect*, **85**, 289–305. (2013).
79. Harrison, R. K. *Nat. Rev. Drug Discov* 817–818. (2016).
80. Sabbagh, J. J., Kinney, J. W. & Cummings, J. L. *Neurobiol. Aging*, **34**, 169–183. (2013).
81. Mak, I. W., Evaniew, N. & Ghert, M. *Am. J. Transl Res.* **6**, 114–118. (2014).
82. Lamotte, J. D. et al. *Front. Pharmacol.*, **11**, 617867. (2020).
83. Morgan, P. et al. *Nat. Rev. Drug Discov* **17**, 167–181. (2018).
84. Calhoun, A., King, C., Khoury, R. & Grossberg, G. T. *Expert Opin. Pharmacother* **19**, 1711–1717. (2018).
85. Chapman, C. A., Nuwer, J. L. & Jacob, T. C. *Front. Synaptic Neurosci.* **14**, 911020. (2022).
86. Gotz, J., Chen, F., Van Dorpe, J. & Nitsch, R. M. *Science*, **293**, 1491–1495. (2001).
87. Lewis, J. et al. *Science*, **293**, 1487–1491. (2001).
88. Calhoun, M. E. et al. *Nature*, **395**, 755–756. (1998).
89. Irizarry, M. C. et al. *J. Neurosci.* **17**, 7053–7059. (1997).
90. Santacruz, K. et al. *Science*, **309**, 476–481. (2005).
91. Yoshiyama, Y. et al. *Neuron*, **53**, 337–351. (2007).
92. Nelson, P. T. et al. *T G Beach Neuropathol. Exp. Neurol.* **71**, 362–381. (2012).
93. Marquez, A. et al. *Neurobiol Dis.* **151**, 105273 (2021).
94. Stecker, M. M., Srivastava, A. & Reiss, A. B. *Int. J. Mol. Sci.* **24**(19), 14488. (2023).
95. Berry, B. J. et al. *Biotechnol. Prog* **31**, 1613–1622. (2015).
96. Wilson, K., Stancescu, M., Das, M., Rumsey, J. & Hickman, J. *J. Vac Sci. Technol. B Nanotechnol Microelectron.* **29**, 21020. (2011).
97. Stine, W. B. Jr., Dahlgren, K. N., Krafft, G. A. & Ladu, M. J. *J. Biol. Chem.* **278**, 11612–11622. (2003).
98. Kuns, B., Rosani, A. & Varghese, D. *In: StatPearls [Internet]* (2021).
99. Dooley, M. & Lamb, H. M. *Drugs Aging*, **16**, 199–226. (2000).
100. Shigeta, M. & Homma, A. *CNS Drug Rev.* **7**, 353–368. (2001).
101. Alzforum *ALZForum*.
102. Tang, S. J. et al. *Acta Neuropathol. Commun.* **8**, 96. (2020).
103. Kaufman, A. C. et al. *Ann. Neurol.* **77**, 953–971. (2015).
104. Nygaard, H. B. *Biol. Psychiatry*, **83**, 369–376. (2018).
105. Garcia-Osta, A., Cuadrado-Tejedor, M., Garcia-Barroso, C., Oyarzabal, J. & Franco, R. *ACS Chem. Neurosci.* **3**, 832–844. (2012).

Acknowledgements

We would like to acknowledge Dr. John Rumsey for his instructive comments on the manuscript.

Author contributions

Conceptualization: KA, XG and JH; data curation: KA, XG, NA, JC, SL; formal analysis: KA, XG, MG, MJ, CL; funding acquisition: JH; investigation and methodology: KA, XG, JH; project administration: XG and JH; supervision: XG and JH; validation: XG, DM and JH; visualization: KA, XG, DM and JH; roles/writing—original draft: KA, XG, JH; writing—review and editing: KA, XG, DM and JH.

Declarations

Competing interests

The authors confirm that competing financial interests exist but there has been no financial support for this research that could have influenced its outcome. JJH has ownership interest and is Chief Scientist and member of the Board of Directors in a company that may benefit financially as a result of the outcomes of the research or work reported in this publication.

Additional information

Supplementary Information The online version contains supplementary material available at https://doi.org/10.1038/s41598-024-73869-9.

Correspondence and requests for materials should be addressed to J.C.

Reprints and permissions information is available at www.nature.com/reprints.

Publisher's note Springer Nature remains neutral with regard to jurisdictional claims in published maps and institutional affiliations.

Open Access This article is licensed under a Creative Commons Attribution-NonCommercial-NoDerivatives 4.0 International License, which permits any non-commercial use, sharing, distribution and reproduction in any medium or format, as long as you give appropriate credit to the original author(s) and the source, provide a link to the Creative Commons licence, and indicate if you modified the licensed material. You do not have permission under this licence to share adapted material derived from this article or parts of it. The images or other third party material in this article are included in the article's Creative Commons licence, unless indicated otherwise in a credit line to the material. If material is not included in the article's Creative Commons licence and your intended use is not permitted by statutory regulation or exceeds the permitted use, you will need to obtain permission directly from the copyright holder. To view a copy of this licence, visit http://creativecommons.org/licenses/by-nc-nd/4.0/.

© The Author(s) 2024